AIP | Journal of Applied Physics

Reordering orbitals of semiconductor multi-shell quantum dot-quantum well heteronanocrystals

Mehmet Şahin, Sedat Nizamoglu, Ozan Yerli, and Hilmi Volkan Demir

Citation: J. Appl. Phys. **111**, 023713 (2012); doi: 10.1063/1.3678585
View online: http://dx.doi.org/10.1063/1.3678585
View Table of Contents: http://jap.aip.org/resource/1/JAPIAU/v111/i2
Published by the American Institute of Physics.

Reordering orbitals of semiconductor multi-shell quantum dot-quantum well heteronanocrystals

Mehmet Şahin,[1,a)] Sedat Nizamoglu,[2] Ozan Yerli,[2] and Hilmi Volkan Demir[2]
[1]*Department of Physics, Faculty of Sciences, Selçuk University, Campus 42075 Konya, Turkey and UNAM-Institute of Materials Science and Nanotechnology, Bilkent University, 06800 Ankara, Turkey*
[2]*Department of Electrical and Electronics Engineering, Department of Physics, and UNAM-Institute of Materials Science and Nanotechnology, Bilkent University, 06800 Ankara, Turkey*

(Received 28 April 2011; accepted 22 December 2011; published online 27 January 2012)

Based on self-consistent computational modeling of quantum dot-quantum well (QDQW) heteronanocrystals, we propose and demonstrate that conduction-electron and valence-hole orbitals can be reordered by controlling shell thicknesses, unlike widely known core/shell quantum dots (QDs). Multi-shell nanocrystals of CdSe/ZnS/CdSe, which exhibit an electronic structure of 1s-1p-2s-2p-1d-1f for electrons and 1s-1p-2s-2p-1d-2d for holes using thin ZnS and CdSe shells (each with two monolayers), lead to 1s-2s-1p-1d-1f-2p electron-orbitals and 1s-2s-1p-1d-2p-1f hole orbitals upon increasing the shell thicknesses while keeping the same core. This is characteristically different from the only CdSe core and CdSe/ZnS core/shell QDs, both exhibiting only 1s-1p-1d-2s-1f-2p ordering for electrons and holes. © *2012 American Institute of Physics*. [doi:10.1063/1.3678585]

I. INTRODUCTION

Quantum confinement (QC) leads to formation of an ordered set of orbitals at discrete energy levels on the conduction and valance bands in semiconductor quantum dots (QDs), which enables strongly size-dependent control of optical properties. Especially when the physical size of a QD is comparable to or smaller than the exciton in its bulk semiconductor material, QC modifies strongly the electronic structure. There exist two commonly known effects of quantum confinement in QDs. The first one is the bandgap modification that results in emission peak shift. For example, QDs made of CdSe span emission color from red to blue by only reducing their size.[1] The second one is the extinction coefficient. The extinction coefficient of QDs per mole rises approximately in a square to cubic function as their size increases.[2]

Quantum dot-quantum wells (QDQW) containing multiple shells have been investigated to seek superior structural properties allowing for strain reduced band engineering. Thus, various material and structure combinations have been studied. The synthesis of CdS/HgS/CdS QDQWs was achieved in 1993,[3] after which CdS/CdSe/CdS and ZnS/CdS/ZnS were successfully synthesized, and some of those QDQW systems were then also theoretically investigated.[4–7] Recently, CdSe/ZnS/CdSe QDQWs have been demonstrated, which advantageously exhibit dual-color emission in ensemble. Both experimentally and theoretically it has been shown that CdSe core and outer shell are coupled via tunneling through ZnS inner shell barrier.[8,9] For application, Sapra *et al*. have investigated white light generation using these QDQW emitters of cyan and red in toluene solution.[10] However, the resulting color rendering was low and QDQWs were not integrated into a solid-state device. Nizamoglu *et al*. have then hybridized such dual-color emitting CdSe/ZnS/CdSe QDQWs on InGaN/GaN light emitting diodes for high-quality white light generation.[11] Furthermore, carrier and spin dynamics in these structures have been investigated and selective initialization and readout of spin using CdSe/ZnS/CdSe QDQWs have been demonstrated.[12] Furthermore, the single dot spectroscopy of these QDQWs has been explored for blinking analysis.[13]

Today it is well known that the quantum mechanical effects become dominant with diminishing dimensions. These effects cater different advantages in operation of the electronic devices. Presently most of the electronic structure and optical properties of quantum dots are theoretically well understood. On the other hand, despite few studies that have been reported in the literature,[7,9,14] the electronic structure and optical properties of QDQWs have not yet been fully understood. Controllable electronic shell structure of multi-layered QDs is important for device applications including tunable color luminophors and multi-color luminophors. The orbital ordering of such QDQWs has not been investigated till date.

In this study, we investigate the shell structure and orbital ordering of multi-layered semiconductor quantum dot-quantum wells made of CdSe/ZnS/CdSe. For that, we use a self-consistent computation of the electronic structure of a single exciton in spherical geometry via matrix diagonalization method. Our results show that electron and hole orbitals of a QDQW can be reordered by varying ZnS and CdSe shell layer thicknesses, in an unusual way different than widely known CdSe/ZnS core/shell QDs. Surprisingly, the orbital reorderings are different for the conduction-electron and valance-hole, depending on shell thickness. These modified electronic structures differ from those of CdSe core and CdSe/ZnS core/shell QDs, which exhibit a typical electronic shell structure of 1s-1p-1d-2s-1f-2p both for electrons and holes. Moreover, we compare overlap integrals, oscillator strengths and absorption coefficients for these QDQWs with various shell thicknesses. The rest of this paper is organized as follows: In Sec. II, model and calculations are presented. Results and discussions are given in Sec. III. A brief conclusion is presented in Sec. IV.

a)Electronic mail: sahinm@selcuk.edu.tr.

II. MODEL AND CALCULATIONS

In this study, a spherically symmetric core/barrier-shell/well-shell/barrier-shell quantum dot structure is considered. As seen from Fig. 1, the core material is chosen as CdSe with radius R_1, which is coated with ZnS barrier shell with a wider bandgap than that of CdSe. This barrier-shell thickness is $R_2 - R_1$. This structure is further coated with CdSe for well-shell region with a thickness of $R_3 - R_2$. Finally, this structure is embedded in ZnS shell material, where thickness of the outmost barrier-shell is $R_4 - R_3$. The effective mass approximation and BenDaniel-Duke boundary conditions are used in the self-consistent calculations. In the effective mass approximation, for a spherically symmetric quantum dot, the single-particle Schrödinger equation is given by

$$\left[-\frac{\hbar^2}{2}\vec{\nabla}_e\left(\frac{1}{m_e^*(r)}\vec{\nabla}_e\right)-\frac{\hbar^2}{2}\vec{\nabla}_h\left(\frac{1}{m_h^*(r)}\vec{\nabla}_h\right)-\frac{e^2}{\kappa|\vec{r}_e-\vec{r}_h|}+V_e+V_h\right]\psi_{n\ell m}^{exc}(\vec{r}_e,\vec{r}_h)=\varepsilon_{n\ell m}\psi_{n\ell m}^{exc}(\vec{r}_e,\vec{r}_h). \tag{1}$$

Here, first two terms are kinetic energy terms of electron and hole, respectively, $\hbar$ is reduced Planck constant, $m_{e,h}^*(r)$ is the position-dependent electron and hole effective masses, e is the unit electronic charge, V_e and V_h are the finite confining potential of the electron and hole, respectively, $\varepsilon_{n\ell m}$ is the exciton energy eigenvalue, and $\psi_{n\ell m}^{exc}(\vec{r}_e,\vec{r}_h)$ is the wavefunction of the exciton.

It is impossible to solve this equation analytically and numerical calculations are hence indispensable. For this purpose, we express Eq. (1) in two pieces separately for electron and hole using Hartree approximation as follows:

$$\left[-\frac{\hbar^2}{2}\vec{\nabla}_r\left(\frac{1}{m_e^*(r)}\vec{\nabla}_r\right)-e\Phi_h+\frac{\ell(\ell+1)\hbar^2}{2m_e^*(r)\,r^2}+V_e\right]R_{n,\ell}^{elec}(r)=\varepsilon_{n,\ell}^{elec}R_{n,\ell}^{elec}(r) \tag{2}$$

and

$$\left[-\frac{\hbar^2}{2}\vec{\nabla}_r\left(\frac{1}{m_h^*(r)}\vec{\nabla}_r\right)-e\Phi_e+\frac{\ell(\ell+1)\hbar^2}{2m_h^*(r)\,r^2}+V_h\right]R_{n,\ell}^{hole}(r)=\varepsilon_{n,\ell}^{hole}R_{n,\ell}^{hole}(r). \tag{3}$$

We should note that our structure and hence the confining potential is spherically symmetric. There is no magnetic field to remove the degeneracy of the level for any ℓ which is different from zero. Hence, there is no a priority for the probability of finding of an electron in a sublevel corresponding to any m_ℓ. Therefore, we can assume that the charge density is spherically symmetric.

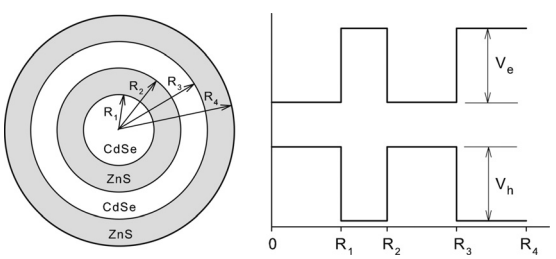

FIG. 1. Schematic representation of a multi-shell spherical quantum dot structure and its potential profile V(r).

In Eq. (2) and Eq. (3), the first terms are kinetic energy terms of the electron and hole, respectively. The second terms represent the attractive Coulomb potential energies between the electron and hole. Here Φ_e and Φ_h are the electrostatic Hartree potential of the electron and hole, respectively. The Hartree approximation used in the formalism supposes that one particle (electron or hole) moves in a mean potential field created by other particle(s) in a many-particle system.[15] ℓ is the angular momentum quantum number and the third term in Eq. (2) and Eq. (3) comes from the angular momentum of the electron and hole. $\varepsilon_{n,\ell}^{elec}$ and $\varepsilon_{n,\ell}^{hole}$ are the respective electron and hole energy eigenvalues; $R_{n,\ell}^{elec}(r)$ and $R_{n,\ell}^{hole}(r)$ are the radial wavefunctions of the electron and hole, respectively.

In this schema, we consider that the electron moves in the electrostatic potential of the hole and similarly the hole moves in the electrostatic potential of the electron. The electron and hole potentials are calculated from the Poisson equation by means of

$$\vec{\nabla}_r\kappa(r)\vec{\nabla}_r\Phi_e=e\rho_e(r), \tag{4}$$

and

$$\vec{\nabla}_r\kappa(r)\vec{\nabla}_r\Phi_h=-e\rho_h(r), \tag{5}$$

where $\rho_e(r)$ is the electron density, $\rho_h(r)$ is the hole density, and $\kappa(r)$ is the position dependent dielectric constant of the structure. The effective masses of electron (hole) inside CdSe and ZnS are m_1^* and m_2^*, and the dielectric constants are κ_1 and κ_2, respectively. The position dependent effective mass and the dielectric constant may be defined as follows:[16,17]

$$m*(r)=\begin{cases}1, & r\le R_1 \quad \text{and} \quad R_2\le r\le R_3,\\ \dfrac{m_2^*}{m_1^*}, & R_1<r<R_2 \quad \text{and} \quad r>R_3,\end{cases}$$
$$\kappa(r)=\begin{cases}1, & r\le R_1 \quad \text{and} \quad R_2\le r\le R_3,\\ \dfrac{\kappa_2}{\kappa_1}, & R_1<r<R_2 \quad \text{and} \quad r>R_3.\end{cases} \tag{6}$$

The electron and hole densities are

$$\rho_e(r)=\frac{1}{4\pi}\sum_{\ell=0}^{p}2(2\ell+1)\sum_{n=1}^{np}|R_{n,\ell}^{elec}(r)|^2+\frac{1}{4\pi}q|R_{nq,\ell q}^{elec}(r)|^2, \tag{7}$$

and

$$\rho_h(r)=\frac{1}{4\pi}\sum_{\ell=0}^{p}2(2\ell+1)\sum_{n=1}^{np}|R_{n,\ell}^{hole}(r)|^2+\frac{1}{4\pi}q|R_{nq,\ell q}^{hole}(r)|^2. \tag{8}$$

Here $2(2\ell+1)$ is the spin and magnetic degeneracies; p and np are the angular momentum quantum number and the

principle quantum number of the fully occupied states, respectively; q is the number of remaining electrons in the last state; nq and ℓq are the principle quantum number and angular momentum quantum number of the last state, respectively. For a single exciton the maximum electron and hole number are $N = 1$ and only one energy state of the conduction and valance bands are occupied with the electron and hole. Therefore, the density of our system is

$$\rho_{e,h}(r) = \frac{1}{4\pi} |R_{n,\ell}^{elec,hole}(r)|^2. \quad (9)$$

The details of the electronic structure calculation and other procedures were presented for a spherical quantum dot without multiple shells in Refs. 17 and 18.

We also investigate the oscillator strength and exciton lifetime in QDQW. The oscillator strength is calculated as follows[19]

$$f = \frac{E_p}{2E_{exc}} \left| \int d^3 r \psi_e(r) \psi_h(r) \right|^2, \quad (10)$$

where E_p is the Kane energy.[20] The electron and hole wavefunctions, $\psi_e(r)$ and $\psi_h(r)$, are obtained by the multiplication of the radial wavefunction determined by Eq. (2) and Eq. (3) with the spherical harmonics (*i.e.*, $R_{n,\ell}(r)Y_{\ell,m}(\theta,\varphi)$). The exciton lifetime is computed by[21,22]

$$\tau = \frac{6\pi\varepsilon_0 m_0 c^3 \hbar^2}{e^2 n \beta_s E^2 f}, \quad (11)$$

where ε_0 is the dielectric permittivity of the vacuum, m_0 is the free electron mass, c is the light velocity, e is the electronic charge, f is the oscillator strength, n is the refractive index, E is the transition energy, and β_s is the screening factor,[22] which is given by

$$\beta_s = \frac{3\varepsilon}{(\varepsilon_{NQD} + 2\varepsilon)}. \quad (12)$$

Here, ε and ε_{NQD} are the optical dielectric constants of the medium solvent and nanocrystal quantum dots, respectively.

III. RESULTS AND DISCUSSION

In this study, we consider wurtzite-type CdSe and ZnS semiconductor material parameters. The atomic units have been used throughout the calculations, where Planck constant $\hbar = 1$, the electronic charge $e = 1$, and the electron mass $m_0 = 1$. By using the material parameters presented in Table I, the effective Bohr radius is found to be $a_0^* = 48.78$ Å and the effective Rydberg energy is calculated to be $R_y^* = 15.86$ meV. The confining potentials of electron and hole are $V_e = 1.05$ eV and $V_h = 0.95$ eV, respectively.[18] 1 monolayer (ML) is taken approximately 0.56 nm for CdSe and approximately 0.50 nm for ZnS.[9]

Figure 2 shows the probability distribution of the electron and hole for 1p, 1d, and 2s states in a QDQW depending on the shell thicknesses. In all graphs, the core radius is chosen as $R_1 = 2.75$ nm. In the figure, X-Y ML means that the thickness of the ZnS shell is X (X = 1, 2, 3) ML and the thickness of the CdSe well is Y (Y = 1, 2, 3) ML. The probability distributions of 1s electron and 1s hole are found to be localized in the core region for all layer thicknesses. Therefore, all optical transitions (both absorption and photoluminescence) occur in the core region similar to those of single core/shell QD structures. On the other hand, as seen from Fig. 2 the probability distributions of other levels (*i.e.*, 1p, 1d, and 2s) exhibit spatially different localization depending on the shell and well thickness. While the electron and hole probability distributions of 1p state are localized in the core region for 1-1 ML, 2-1 ML, and 3-2 ML structures, the electron probability is more localized in the well region for 1-3 ML and both electron and hole distributions are just about to be completely localized in the well region for 2-3 ML and 3-3 ML structures. In the case of 1p, shown in the top panels of the figure, although the optical processes take place in the core for 1-1, 1-2, 2-1, 2-2, 3-1, and 3-2 ML, these occur in the well region for 2-3 and 3-3 ML. For the case of 1-3 ML, strong absorption or efficient photoluminescence is not expected because of the weak overlapping. When we focus on the 1d case shown in the middle panel of Fig. 2, we see that the optical transitions happen in the core for 1-1, 2-1 and 3-1 ML and in the well for 1-3, 2-3, 3-2, and 3-3 ML. On the other hand, for 1-2 and 2-2 ML, since the electron confines in the well region and the hole confines in the core region, leading to weak transition, there is probably no strong transition. In the bottom panel of Fig. 2, the density probability distributions of the electron and hole are depicted for 2s. In this case, the hole confines in the core for 1-1, 2-1, and 3-1 ML. But the electron is confined in the well region for these layer thicknesses because of its light effective mass. In this situation, the overlap of the electron and hole wavefunctions is poor and hence the optical transitions will be rather poor. On the other hand, for other layer thicknesses the electron and hole probability distributions are both localized in the well especially for the cases of 2-2, 2-3, 3-2, and 3-3 ML and their transitions will occur in this layer. As a result of these electronic structures, we conclude that, in single exciton regime, the optical transitions (both absorption and luminescence) occur either in the core alone or in the well alone.

As it is well known, there are two principle optical transitions in a QD, interband and intraband transitions. In some QD structures, e.g., those produced from II-VI group, the intraband transitions take place in the mid or far-infrared region, whereas the interband transitions occur in the visible region. Therefore, the QDs made of II-VI group offer important technological uses and hence, understanding physics of these structures is essential. When a photon is absorbed in a QD, this process results in an electron transition from the valance band to the conduction band. Of course this interband transition processes can take place between 1s-1s, 1p-1p, 1d-1d, and so on, depending on the selection rules.

TABLE I. The material parameters used in the calculations.

Material	m_e* (Ref. 23)	m_h* (Ref. 9)	κ (Ref. 23)	E_g (eV) (Ref. 23)
CdSe	$0.13m_0$	$0.45m_0$	9.3	1.75
ZnS	$0.28m_0$	$0.49m_0$	8.1	3.75

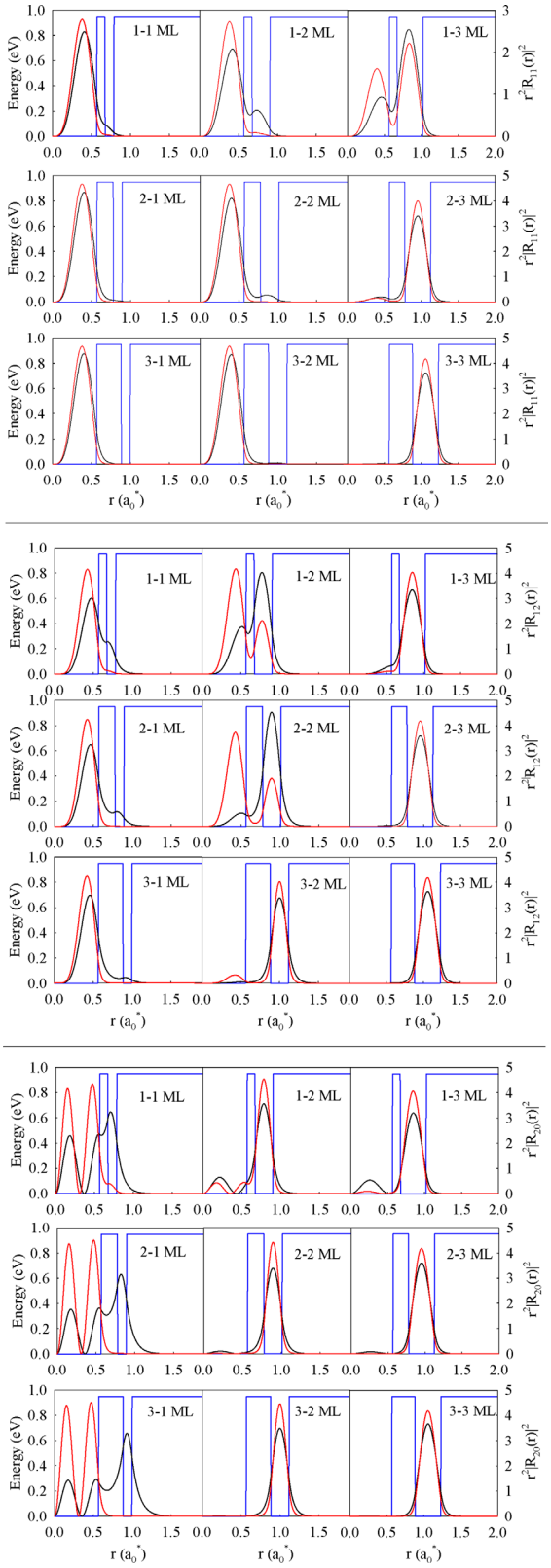

FIG. 2. (Color online) Probability distribution of an electron and a hole in a multi-shell spherical quantum dot structure for 1p states (top panel), 1d states (middle panel), and 2s states (bottom panel). The blue lines correspond to potential profile, black lines correspond to the electron probability distribution, and red lines correspond to the hole probability distribution.

Therefore, the shell structure of QD nanocrystals plays a key role for possible device applications. The common shell structure of a single core/shell QD is 1s, 1p, 1d, 2s, 1f, 2p, … for both electrons and holes. On the other hand, in a multilayered QD, the electronic shell structure can be reordered depending on layer thicknesses, unlike a simple QD. In Table II, reordering of the electron and hole orbitals is presented. As seen from the table, for all different layer thicknesses, the shell structure exhibits different ordering. For example, in 1-3 ML structure, the first six shell structures of the electron are 1s, 1p, 2s, 1d, 1f, and 2p, while those of the hole are 1s, 2s, 1p, 1d, 2p, and 1f.

TABLE II. The shell structure and orbital ordering of QDQWs for the electron and hole given different shell thicknesses.

Struc. (ML)	Elec.	Hole	Struc. (ML)	Elec.	Hole	Struc. (ML)	Elec.	Hole
	1s	1s		1s	1s		1s	1s
	1p	1p		1p	1p		1p	2s
1-1	1d	1d	1-2	2s	2s	1-3	2s	1p
	2s	2s		1d	1d		1d	1d
	2p	1f		2p	2p		1f	2p
	3s	2p		1f	2d		2p	1f
	1s	1s		1s	1s		1s	1s
	1p	1p		1p	1p		2s	2s
2-1	2s	1d	2-2	2s	2s	2-3	1p	1p
	1d	2s		2p	2p		1d	1d
	2p	1f		1d	1d		1f	2p
	3s	2p		1f	2d		2p	1f
	1s	1s		1s	1s		1s	1s
	1p	1p		1p	1p		2s	2s
3-1	2s	1d	3-2	2s	2s	3-3	1p	1p
	1d	2s		2p	2p		1d	1d
	2p	1f		1d	1d		1f	2p
	1f	2p		1f	2d		2p	1f

The electronic structure and optical properties of 1s, 1p, 1d, and 2s single excitons are presented depending on the combinations of layer thicknesses in Tables III, IV, V, and VI, respectively. Here, the absorption wavelength corresponds to resonant cases and the binding energy corresponds to the attractive Coulomb potential energy between the electron and hole. The oscillator strength and the exciton lifetime are computed by Eq. (10) and Eq. (11), respectively. As presented in Table III, the 1s exciton binding energies and oscillator strengths decrease in 1-Y ML structures with increasing

TABLE III. Electronic and optical properties computed for 1s exciton.

Structure (ML)	Binding energy (eV)	Absorption wavelength (nm)	Oscillator strength	Exciton lifetime (ns)
1-1	0.0782	608	5.075	1.31
1-2	0.0769	609	5.049	1.32
1-3	0.0742	611	4.969	1.35
2-1	0.0792	606	5.080	1.30
2-2	0.0791	607	5.076	1.30
2-3	0.0788	607	5.065	1.30
3-1	0.0793	606	5.082	1.30
3-2	0.0793	606	5.082	1.30
3-3	0.0793	606	5.081	1.30

TABLE IV. Electronic and optical properties computed for 1p exciton.

Structure (ML)	Binding energy (eV)	Absorption wavelength (nm)	Oscillator strength	Exciton lifetime (ns)
1-1	0.0613	514	4.162	1.14
1-2	0.0551	520	3.886	1.25
1-3	0.0303	539	4.313	1.21
2-1	0.0632	510	4.199	1.11
2-2	0.0606	511	4.043	1.16
2-3	0.0216	528	4.385	1.14
3-1	0.0636	509	4.217	1.10
3-2	0.0631	510	4.187	1.11
3-3	0.0182	528	4.385	1.14

Y (Y = 1, 2, 3). The absorption wavelength tends to increase with increasing Y. However, there are no drastic changes in the exciton lifetimes and similar situation appears in 2-Y ML structures. On the other hand, in 3-Y ML structure, the results are all the same for three Y values. In 1-Y ML structures, although the electron and hole confine in the core region, they are affected from the well region because the shell thickness is 1 ML. In 2-Y ML case, the shell thickness is 2 ML and the electron and hole are affected comparatively less. When the shell thickness becomes 3 ML (*i.e.*, 3-Y ML), the electron and hole do not feel the well region. Hence, all of the calculation results are the same with each other for 3-Y, unlike 1-Y and 2-Y. In this case, the structure exhibits completely single QD properties.

When we look at the electronic structure and optical properties for 1p and 1d excitons presented in Table IV and Table V, respectively, we observe different behavior from the case of 1s. As seen in these tables, the binding energy of 1p exciton is greater than that of 1d exciton and this energy is strongly dependent on the well thickness. As the well thickness increases, the binding energy decreases in both 1p and 1d. In addition, the absorption band edge shifts to longer wavelengths with increasing well thickness. However, in both cases, the oscillator strength and the exciton lifetime do not depend monotonically on the shell thickness. Physical reason of this observation can be explained by looking at Fig. 2. In the top and middle panels of the figure, the probability distribution of the electron localized especially in the well region with increasing Y while the hole is confined in the core region. Therefore, the binding

TABLE V. Electronic and optical properties computed for 1d exciton.

Structure (ML)	Binding energy (eV)	Absorption wavelength (nm)	Oscillator strength	Exciton lifetime (ns)
1-1	0.0499	443	3.087	1.14
1-2	0.0355	464	3.183	1.21
1-3	0.0253	512	4.231	1.11
2-1	0.0512	435	3.048	1.12
2-2	0.0272	456	2.267	1.65
2-3	0.0212	513	4.251	1.11
3-1	0.0529	433	3.207	1.05
3-2	0.0204	456	3.559	1.05
3-3	0.0181	516	4.291	1.11

TABLE VI. Electronic and optical properties computed for 2s exciton.

Structure (ML)	Binding energy (eV)	Absorption wavelength (nm)	Oscillator strength	Exciton lifetime (ns)
1-1	0.0544	430	2.279	1.45
1-2	0.0302	472	3.741	1.07
1-3	0.0256	533	4.207	1.21
2-1	0.0472	422	1.582	2.02
2-2	0.0238	471	3.789	1.05
2-3	0.0213	534	4.406	1.16
3-1	0.0402	419	1.216	2.59
3-2	0.0202	470	3.806	1.04
3-3	0.0182	534	4.444	1.15

energies are smaller in thicker wells. By expanding the well region, the quantum confinement effect becomes weaker and the absorption band edge wavelength increases (*i.e.*, transition energies decrease). However, as seen from Eq. (10), since the oscillator strength depends on both transition energy and overlap of the electron and hole wavefunctions, its change is not monotonical. For example, although the transition energy of 1p exciton in the 1-2 ML structure is larger than that of 1-3 ML structure, the oscillator strength of the 1-2 ML structure becomes weaker compared to that of 1-3 ML because the overlap of the corresponding wavefunctions is larger in 1-3 ML structure. Similar argument is valid for the exciton lifetimes calculated by Eq. (11).

In 2s exciton, as observed in Table VI, while the binding energies and the absorption peak wavelengths monotonically decrease with the increased barrier and well shell thickness, the oscillator strength increases. However, the modifications in the exciton lifetimes are not uniform. The transitions take place approximately in the far blue region in X-1 ML structures and this region shifts toward the visible region boundary in 3-1 ML structure. Nevertheless, the oscillator strengths of these transitions are rather small because the electron confines in the well and the hole confines in the core as seen from the bottom panels of Fig. 2 and, hence, the overlap integral of the electron and hole wavefunctions is small.

The single exciton absorption processes in a single core/shell QD, all possible transitions of 1s-1s, 1p-1p, 1d-1d, and so on, take place between the valance and conduction bands. However, this does not mean the photoluminescence processes will occur in the same order. When a photon interacts with a QD, a 1p electron in the valance band makes a vertical transition to the 1p state in the conduction band by absorbing this photon. In intersublevel transition mechanisms, the selection rule is $\Delta\ell = \pm 1$ and the relaxation time is approximately order of 10^{-12} *s*.[24,25] Therefore, the probability of the electron transition between intersublevels is larger than that of the transition between the conduction and valance band. As a result, the 1p electron will first relax down to 1s level in the conduction band (similarly, with the hole relaxing to 1s level of the valance band) and then this exciton will recombine from 1s states. Hence, although the absorption occurs between 1p-1p states, the photoluminescence (radiative recombination) take place between 1s-1s states. Therefore, even if there are multi-exciton (*i.e.*, biexciton or three excitons) in a simple

QD structure, multicolor emission will not be produced from higher energy levels because of this intersublevel transitions.

In QDQW however, the optical transitions can be controlled by tuning the shell thicknesses and also photons at different wavelengths can be produced with multiexciton process. 1s state is always ground level in all spherical QD structures. However, the other states can be tuned by adjusting shell thicknesses. When the orbital ordering becomes 1s, 2s for 2-3 or 3-3 ML structures as seen from Table II, an electron makes a transition from 1p of the valance band to 1p of the conduction band, this electron then relaxes to 2s level in the conduction band. Similar process occurs in the valance band. As a result, the recombination process takes place between 2s-2s levels. Resultantly, dual-color emission can be produced in such QDQW heteronanocrystals.

IV. CONCLUSION

In this study, we have carried out a systematic study of electronic shell structure and optical properties of a quantum dot-quantum well heterostructures. We have demonstrated that the electronic shell structure of such QDQW heteronanocrystals (and hence the optical properties) can be controlled by tuning the layer thicknesses. We proposed that this provides the ability to control photoluminescence, for example, dual-color emission. We believe that this study will stimulate different experimental studies related to the design of electronic states in QDQWs.

ACKNOWLEDGMENTS

This study was supported by TUBITAK TBAG with Project No. 109T729. One of the authors (M.Ş.) thanks Selçuk University BAP office for their partial financial support and also, Marmaris Institute of Theoretical and Applied Physics (ITAP) for hospitality. Three of the authors (H.V.D, S.N., and O.Y.) acknowledge the support from ESF EURYI, TÜBA-GEBİP and EU FP7 N4E NoE.

[1]A. P. Alivisatos, Science **271**, 933 (1996).
[2]W. W. Yu, L. Qu, W. Guo, and X. Peng, Chem. Mat. **15**, 2854 (2003).
[3]A. Eychmller, A. Mews, and H. Weller, Chem. Phys. Lett. **208**, 59 (1993).
[4]R. B. Little, M. A. El-Sayed, G. W. Bryant, and S. J. Burke, J. Chem. Phys. **114**, 1813 (2001).
[5]S. A. Ivanov, J. Nanda, A. Piryatinski, M. Achermann, L. P. Balet, I. V. Bezel, P. O. Anikeeva, S. Tretiak, and V. I. Klimov, J. Phys. Chem. B **108**, 10625 (2004).
[6]X. Zhong, R. Xiea, Y. Zhang, T. Basch, and W. Knoll, Chem. Mater. (Communication) **17**, 4038 (2005).
[7]J. Schrier and L. Wang, Phys. Rev. B **73**, 245332 (2006).
[8]E. A. Dias, S. L. Sewall, and P. J. Kambhampati, Phys. Chem. C **111**, 708 (2007).
[9]S. Nizamoglu and H. V. Demir, Optics Express **16**, 3515 (2008).
[10]S. Sapra, S. Mayilo, T. A. Klar, A. L. Rogach, and J. Feldmann, Adv. Mater. **19**, 569 (2007).
[11]S. Nizamoglu, E. Mutlugun, T. Ozel, H. V. Demir, S. Sapra, N. Gaponik, and A. Eychmuller, Appl. Phys. Lett. **92**, 113110 (2008).
[12]J. Berezovsky, O. Gywat, F. Meier, D. Battaglia, X. Peng, and D. D. Awschalom, Nat. Phys. **2**, 831 (2006).
[13]E. A. Dias, A. F. Grimes, D. S. English, and P. Kambhampati, J. Phys. Chem. C **112**, 14229 (2008).
[14]K. Chang and J.-B. Xia, Phys. Rev. B **57**, 9780 (1998).
[15]E. A. Johson, in *Low Dimensional Semiconductor Structures,* edited by K. Barnham and D. Vvedensky (Cambridge University Press, Cambridge, 2001), p. 79.
[16]R. Buczko and F. Bassani, Phys. Rev. B **54**, 2667 (1996).
[17]M. Şahin, Phys. Rev. B **77**, 045317 (2008).
[18]M. Şahin, S. Nizamoglu, A. E. Kavruk, and H. V. Demir, J. Appl. Phys. **106**, 043704 (2009).
[19]J. H. Davies, *The Physics of Low-Dimensional Semiconductors: An Introduction* (Cambridge University Press, Cambridge, 1996).
[20]E. W. Van Stryland, M. A. Woodall, H. Vanherzeele, and M. J. Soileau, Opt. Lett. **10**, 490 (1985).
[21]M. Califano, A. Franceschetti, and A. Zunger, Phys. Rev. B **75**, 115401 (2007).
[22]B. Alen, J. Bosch, D. Granados, J. Martinez-Pastor, J. M. Garcia, and L. Gonzalez, Phys. Rev. B **75**, 045319 (2007).
[23]S. Adachi, *Properties of Group-IV, III-V and II-VI Semiconductors* (Wiley, Chichester, 2005).
[24]P. Bhattacharya, X. Su, S. Chakrabarti, A. D. Stiff-Roberts, and C. H. Fischer, in "Intersubband Transitions in Quantum Dots," edited by R. Paiella, *Intersubband Transitions in Quantum Structures* (McGraw-Hill,, New York, 2006).
[25]P. Guyot-Sionnest, M. Shim, and C. Wang, in "Intraband Spectroscopy and Dynamics of Colloidal Semiconductor Quantum Dots," *Nanocrystal Quantum Dots,* edited by V. I. Klimov (CRC, Boca Raton, 2010).